Polybasic RKKR motif in the linker region of lipid droplet (LD)–associated protein CIDEC inhibits LD fusion activity by interacting with acidic phospholipids

Received for publication, July 20, 2018, and in revised form, October 24, 2018 Published, Papers in Press, October 25, 2018, DOI 10.1074/jbc.RA118.004892

Jia Wang[‡], Chengsong Yan[§], Chenqi Xu[§], Boon Tin Chua[¶], Peng Li[‡1], and Feng-Jung Chen[‡¶2]

From the [‡]State Key Laboratory of Membrane Biology and Tsinghua-Peking Center for Life Sciences, Beijing Advanced Innovation Center for Structural Biology, School of Life Sciences, Tsinghua University, Beijing 100084, the [§]State Key Laboratory of Molecular Biology, Shanghai Science Research Center, CAS Center for Excellence in Molecular Cell Science, Shanghai Institute of Biochemistry and Cell Biology, Chinese Academy of Sciences, University of Chinese Academy of Sciences, 320 Yueyang Road, Shanghai 200031, and the [¶]Institute of Metabolism and Integrative Biology, Fudan University, Shanghai 200438, China

Edited by George M. Carman

Lipid droplets (LDs) are intracellular organelles and a central site for lipid synthesis, storage, and mobilization. The size of LDs reflects the dynamic regulation of lipid metabolism in cells. Previously, we found that cell death–inducing DFFA-like effector C (CIDEC) mediates LD fusion and growth by lipid transfer through LD–LD contact sites in adipocytes and hepatocytes. The CIDE-N domains of CIDEC molecules form homodimers, whereas the CIDE-C domain plays an important role in LD targeting and enrichment. Here, using targeted protein deletions and GFP expression coupled with fluorescence microscopy, we identified a polybasic RKKR motif in the linker region that connects the CIDE-N and CIDE-C domains of CIDEC and functions as a regulatory motif for LD fusion. We found that deletion of the linker region or mutation of the RKKR motif increases the formation of supersized LDs compared with LD formation in cells with WT CIDEC. This enhanced LD fusion activity required the interaction between CIDE-N domains. Mechanistically, we found that the RKKR motif interacts with acidic phospholipids via electrostatic attraction. Loss of this motif disrupted the protein–lipid interaction, resulting in enhanced lipid droplet fusion activity and thus formation of larger LDs. In summary, we have uncovered a CIDEC domain that regulates LD fusion activity, a finding that provides insights into the inhibitory regulation of LD fusion through CIDEC–lipid interactions.

Lipid droplets (LDs)[3] consist of the neutral lipid core surrounded by a monolayer of phospholipids and LD-associated proteins (1). The excessive storage of neutral lipids in LDs is closely associated with the development of obesity, type II diabetes, cardiovascular diseases, fatty liver diseases, and neurodegeneration (2–7). Nascent LDs that budded from the endoplasmic reticulum (ER) (8–11) continue to grow and mature via one of three processes, namely triglyceride (TAG) synthesis within LD (12), lipid transfer from the ER to LD through contact (13–15), or LD fusion (16–18). The LD fusion process is mediated by the cell death–inducing DFFA-like effector (CIDE) family proteins that include CIDEA, CIDEB, and CIDEC/Fsp27 (19, 20).

CIDEA is highly expressed in brown adipose tissue (BAT) and regulates LD size and lipid storage (21). Under a high-fat diet condition, CIDEA expression is greatly elevated in the liver of mice, leading to severe nonalcoholic fatty liver disease (22). CIDEB is mainly expressed in the liver and small intestine of mice (23–25). *Cideb*-knockout mice are resistant to high-fat diet–induced liver steatosis (23, 25). CIDEC is highly expressed in white adipose tissue (WAT). Concomitantly, the adipocytes of *Cidec*$^{-/-}$ mice exhibit small multilocular LDs, reduced triglyceride storage, and increased lipolysis (26, 27). A patient with a homozygous nonsense mutation in *Cidec* also exhibits small multilocular LDs in adipocytes and suffers from severe metabolic syndromes such as insulin resistance and partial lipodystrophy (28). In addition, the combination therapy that utilized antisense oligonucleotide to silence *Cidec* and *fenofibrate* (peroxisome proliferator-activated receptor-α agonist) has proven to ameliorate obesity, hypertriglyceridemia, hepatic steatosis, and inflammation induced by a high-fat diet in mouse models (29, 30). Mechanistically, CIDE family proteins are enriched at the LD–LD contact sites (LDCSs) enabling lipid transfer to occur between two LDs (16, 20, 31, 32), thus promoting LD fusion and growth in BAT, WAT, and the liver.

Previously, we reported that CIDEC mediates LD fusion by means of directional lipid transfer from smaller (donor) to larger (acceptor) LDs (16). The enrichment of CIDEC at LDCS is a prerequisite for LD fusion prior to fusion pore formation. The latter is an essential step for lipid transfer to occur. Molec-

This work was supported by National Basic Research Program Grants 2018YFA0506901 and 2016YFA0502002 (to P. L.) and National Natural Science Foundation of China Grants 31430040, 31690103, and 31621063 (to P. L.). The authors declare that they have no conflicts of interest with the contents of this article.

This article contains Figs. S1–S3.

[1] To whom correspondence may be addressed. Tel.: 86-10-62797121; E-mail: li-peng@mail.tsinghua.edu.cn.

[2] To whom correspondence may be addressed. Tel.: 86-10-62797121; E-mail: derrick.eo93g@gmail.com.

[3] The abbreviations used are: LD, lipid droplet; CIDE, cell death–inducing DFFA-like effector; LDCS, LD–LD contact site; TAG, triglyceride; ANOVA, analysis of variance; PA, phosphatidic acid; PI, phosphatidylinositol; PS, phosphatidylserine; PC, phosphatidylcholine; PE, phosphatidylethanolamine; LUV, large unilamellar vesicle; aa, amino acid; OA, oleic acid; ER, endoplasmic reticulum; FRAP, fluorescence recovery after photobleaching; CHX, cycloheximide; DIC, differential interference contrast.

ularly, on CIDEC, there is a conserved N-domain (CIDE-N) and a C-domain (CIDE-C) joined by a stretch of a 16-amino acid linker. The mechanistic study showed that the CIDE-C domain of CIDEC is responsible for LD targeting; in particular, aa 136–217 are crucial for CIDEC enrichment at the LDCS (16). Other studies have also demonstrated the significance of the CIDE-C domain in LD fusion (33, 34). The CIDE-N domain of CIDEC does not localize on the LD surface and has a regulatory function in promoting LD growth (16, 17). The crystal structure of the CIDE-N domain, including aa 39–119, has been resolved (17, 35). The structure revealed the formation of a homodimer between two CIDEC proteins through the interaction of their CIDE-N domains. CIDEC proteins also interact with Perilipin1 (PLIN1), an activator of CIDEC-mediated LD fusion via the CIDE-N domain (17).

In the last few years, lipidomics study in mammalian cells revealed that phosphatidylcholine (PC) is the most abundant component of the phospholipids on LD. Other minor components include phosphatidylethanolamine (PE), phosphatidylinositol (PI), phosphatidylserine (PS), and ether-linked PC (36, 37). PC on LD serves as the protective agent, preventing LD coalescence due to its cylindrical shape (38). However, it is phosphatidic acid (PA) that was reported to facilitate LD fusion (39, 40). In fact, acidic phospholipids cluster on focal points of ~11 nm in diameter on the plasma membrane and associate with caveolae structures of 60–80 nm (41, 42). In addition, several groups have recently shed light on the protein structure and functional regulation through ionic interactions between proteins and lipids (43–45).

Here, we identified a unique function of CIDEC linker, which connects the CIDE-N and CIDE-C domain. This linker, in particular the polybasic RKKR motif, serves as an inhibitory domain, reducing LD fusion activity, regulating the sizes of LDs. The inhibitory function requires the interaction between CIDE-N domains in a different manner from PLIN1 activation. Mechanistically, the RKKR motif interacts with acidic phospholipids electrostatically. These data reveal a novel functional domain and provide evidence for the synergistic outcome of CIDE-N and CIDE-C domains in regulation of LD fusion and growth by interaction with phospholipids.

Results

Linker region of CIDEC inhibits LD fusion and growth

CIDEC comprises the CIDE-N and CIDE-C domains, connected through a linker region (Fig. 1*A*). The function of the linker, including aa 120–135, remains unknown. Here, we seek to understand the role of the linker domain on CIDEC by first studying the LD phenotype upon 16-aa (linker) deletion. Full-length CIDEC and CIDEC with linker deletion (Δ120–135) were both tagged with GFP on the C terminus and overexpressed in 3T3-L1 pre-adipocytes. Cells expressing full-length CIDEC presented larger Bodipy C12-stained LDs compared with the GFP-expressing cells (Fig. 1*B*). Interestingly, in CIDEC(Δ120–135)–GFP-expressing cells, larger and fewer LDs were found in contrast to LDs in full-length CIDEC–GFP-expressing cells (Fig. 1*B*). In the images acquired, the localization of CIDEC(Δ120–135)–GFP was similar to that of full-length CIDEC with the green fluorescent signals enriched at LDCS (Fig. 1, *B* and *C*). Next, ~100 images of GFP-positive cells were acquired, and the diameter of the largest LD in each cell was measured (Fig. 1*D*). As expected, full-length CIDEC expression mediated LD fusion as shown with the larger average LD diameter compared with the control GFP-expressing cells (3.8 ± 1.3 μm *versus* 0.7 ± 0.2 μm, respectively). Supporting the imaging data, in the absence of the linker, the average size of the largest LD was ~1.5× larger than that of the LDs in cells expressing full-length CIDEC (5.4 ± 1.9 μm, Fig. 1*D*). For easy characterization, LDs with a diameter larger than 4 μm were defined as supersized LDs. The classification of LDs showed that 76% of CIDEC(Δ120–135)–GFP-expressing cells exhibited supersized LDs (Fig. 1*E*). In contrast, only 38% of full-length CIDEC–GFP-expressing cells contained supersized LDs (Fig. 1*E*). Moreover, there were significantly fewer LDs in cells overexpressing CIDEC(Δ120–135)–GFP (10 ± 10 LDs) as compared with cells expressing full-length CIDEC (21 ± 19 LDs) or GFP (296 ± 162 LDs) (Fig. 1*F*). The results indicate that CIDEC(Δ120–135) can further promote LD fusion and growth.

To understand the enlarged LD phenotype in the presence of CIDEC(Δ120–135), we next analyzed the neutral lipid exchange between LDs using fluorescence recovery after photobleaching (FRAP) (16, 17). This is a surrogate assay to demonstrate the opening status of the fusion pore during LD fusion. Here, a significantly shorter signal recovery time was observed for the LD pairs of CIDEC(Δ120–135)-expressing cells (11.2 s for CIDEC(Δ120–135) *versus* > 56 s for full-length CIDEC) (Fig. 1*G*). Quantitative analysis showed that the lipid-exchange rate between LD pairs for CIDEC(Δ120–135)–GFP (2.87 ± 2.03 μm^3/s) was 6.5-fold faster than that for full-length CIDEC–GFP (0.44 ± 0.45 μm^3/s) (Fig. 1*H*). Next, we visualized and measured LD fusion process using time-lapse differential interference contrast (DIC) imaging. It is noted that without the 16-aa linker, LD fusion was completed in a much shorter time of 58 min for a donor LD of 3 μm in diameter, compared with 198 min for similarly-sized LD pairs in cells expressing full-length CIDEC (Fig. 1*I*). Statistically, the lipid transfer rate assay demonstrated that CIDEC(Δ120–135)–GFP-induced neutral lipid transfer rate was 4.4-fold faster than that of full-length CIDEC in average (0.018 ± 0.014 μm^3/min for full-length CIDEC *versus* 0.079 ± 0.054 μm^3/min for CIDEC(Δ120–135)) (Fig. 1*J*). Importantly, there is no change in the total volume of LDs in CIDEC(Δ120–135)-expressing cells with enhanced LD fusion phenotype (Fig. S1*A*). These data indicate that the absence of linker has no effect on total TAG content in 3T3-L1 pre-adipocytes in this short experimental period of 20–24 h. Thus, quantitatively, we uncover that the linker region (aa 120–135) significantly regulates LD fusion activity.

Interaction between CIDE-N domains is required for the enhanced LD fusion phenotype mediated by CIDEC(Δ120–135)

The striking LD phenotype caused by the deletion of the 16-aa linker is evident. Because CIDEC proteins homodimerized via the CIDE-N domain as they enriched at LDCS, we ask whether this homodimerization is required for the enhanced LD fusion mediated by CIDEC(Δ120–135). Using

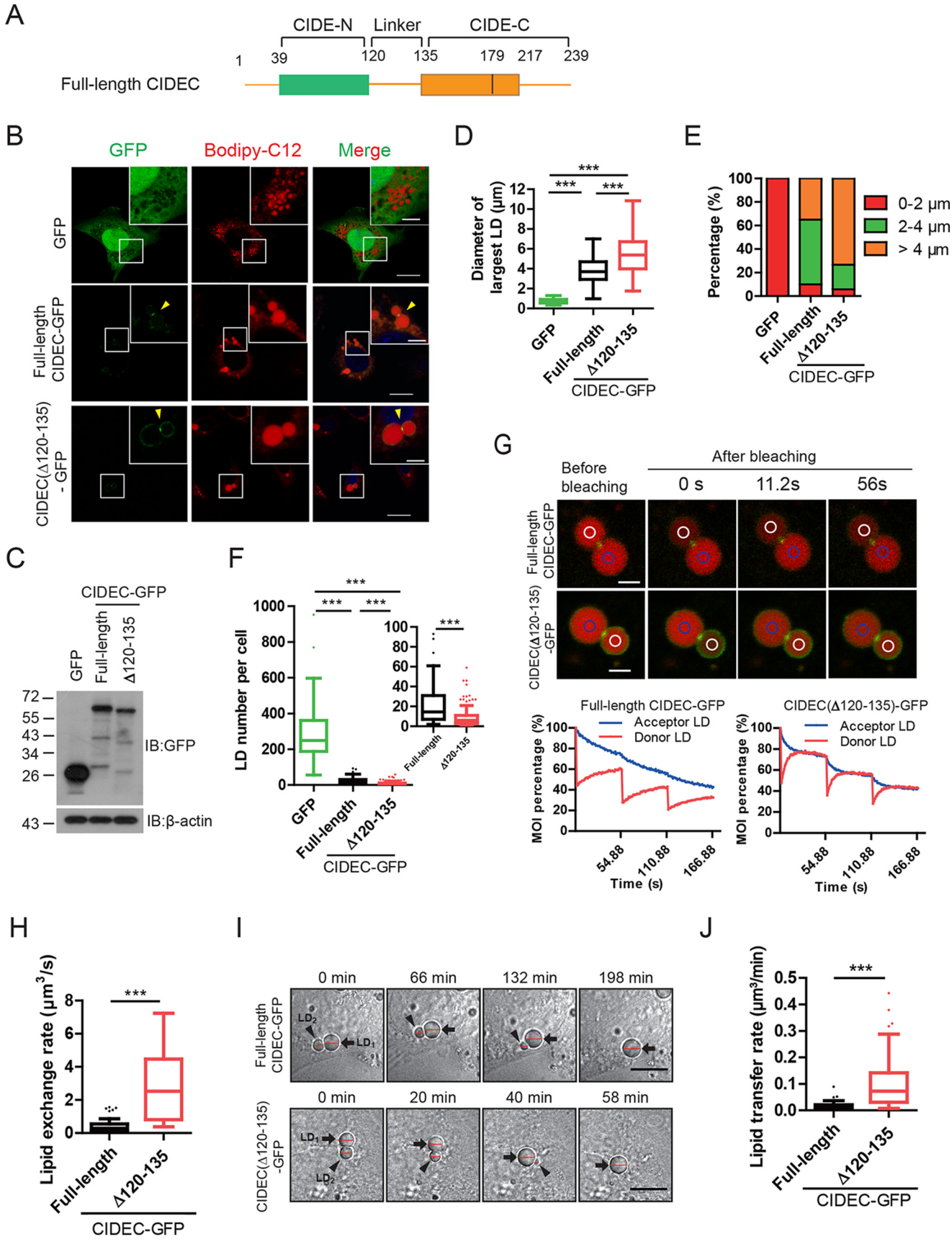
A
CIDE-N
Linker
CIDE-C
1
39
120
135
179
217
239
Full-length CIDEC
B
GFP
Bodipy-C12
Merge
GFP
Full-length CIDEC-GFP
CIDEC(Δ120-135) - GFP
C
CIDEC-GFP
GFP
Full-length
Δ120-135
72
55
43
34
26
IB:GFP
43
IB:β-actin
D
Diameter of largest LD (μm)
***
***
***
GFP
Full-length
Δ120-135
CIDEC-GFP
E
Percentage (%)
0-2 μm
2-4 μm
> 4 μm
GFP
Full-length
Δ120-135
CIDEC-GFP
F
LD number per cell
***
***
***
***
Full-length
Δ120-135
GFP
Full-length
Δ120-135
CIDEC-GFP
G
Before bleaching
After bleaching
0 s
11.2s
56s
Full-length CIDEC-GFP
CIDEC(Δ120-135) -GFP
Full-length CIDEC-GFP
Acceptor LD
Donor LD
MOI percentage (%)
54.88
110.88
166.88
Time (s)
CIDEC(Δ120-135)-GFP
Acceptor LD
Donor LD
MOI percentage (%)
54.88
110.88
166.88
Time (s)
H
Lipid exchange rate (μm³/s)
***
Full-length
Δ120-135
CIDEC-GFP
I
0 min
66 min
132 min
198 min
Full-length CIDEC-GFP
LD2
LD1
0 min
20 min
40 min
58 min
CIDEC(Δ120-135) -GFP
LD1
LD2
J
Lipid transfer rate (μm³/min)
***
Full-length
Δ120-135
CIDEC-GFP

immunoprecipitation assay, the data showed successful pull-down of CIDEC(Δ120–135), with levels comparable with full-length CIDEC (Fig. 2*A*). In addition, in the cycloheximide (CHX) time-chase experiment, CIDEC(Δ120–135) and full-length CIDEC displayed a similar degradation rate (Fig. 2*B*). The results reveal that promotion of supersized LDs via deletion of the linker on CIDEC was not due to stronger interaction between the mutant proteins or enhanced protein stability. Taken together, the increased LD fusion rate induced by CIDEC(Δ120–135) is neither the result of enhanced protein–protein interaction nor increased protein level.

Next, we ask whether the linker collaborates with the N- and C-domains intramolecularly. A number of different CIDEC deletion and mutation plasmids were constructed and examined in the pre-adipocytes (Fig. 2*C*). These constructs include the CIDEC QQN mutant and several N- and C-terminal truncations. The former is defective in N-terminal interaction (QQN-CIDEC) and thus is impaired in LD fusion. Co-expression of PLIN1 can rescue this deficiency through its interaction with the CIDE-N domain (17). With these constructs, lipid-exchange rates were measured and compared between full-length CIDEC, CIDE-N domain (aa 120–239) truncation, and CIDE-N-linker deletion (aa 136–239) (Fig. 2*C*). Data showed that in the absence of CIDE-N, regardless of the presence of linker, lipid-exchange rates were significantly reduced (0.40 ± 0.34 $\mu m^3/s$ for full-length CIDEC; 0.24 ± 0.18 $\mu m^3/s$ for N-domain– deleted CIDEC; and 0.15 ± 0.12 $\mu m^3/s$ for N-domain and linker-deleted CIDEC) (Fig. 2, *D* and *E*). This is unlike the enhanced lipid-exchange rate observed when only the linker was deleted in Fig. 1*H*. The data indicate that the promotion of LD fusion via deletion of the linker region requires the presence of the CIDE-N domain. Next, we asked whether a functional CIDE-N is important. Using the QQN mutant that is defective in homodimerization, an additional 16-aa deletion was constructed (QQN-CIDEC(Δ120–135)). The lipid-exchange assay performed showed that the absence of the linker region could not rescue the low lipid-exchange rate between LDs in the cells expressing CIDEC with the defective CIDEC-N domain (Fig. 2*F*). Our data imply that a functional N-domain is a prerequisite for the regulatory role of the linker. Interestingly, when PLIN1 was co-expressed with QQN-CIDEC(Δ120–135), the exchange rate was increased significantly compared with the cells co-expressing QQN-CIDEC with PLIN1 (Fig. 2, *F* and *G*). This indicates that the deletion of the linker region could recover its promotion for LD fusion so long as PLIN1 can rescue the N-terminal defect of QQN-CIDEC. These data suggest that the regulatory effect of the CIDEC linker on LD fusion is a downstream step after N-domain dimerization.

RKKR motif in the linker regulates LD size

To identify possibly conserved amino acids in the linker responsible for the LD size regulation, we compared the sequences of human and murine CIDE family proteins corresponding to this domain (aa 120–135 of murine CIDEC) (Fig. S1*B*). Our analysis revealed low conservation among the six proteins. To determine whether the linker of other members of the CIDE family has similar restrictions on LD fusion and growth, we compared the LD sizes in cells expressing murine full-length CIDEA–GFP, CIDEA(Δ112–120)–GFP, and CIDEA(Δ112–125)–GFP. Interestingly, instead of enhancing LD fusion and growth, the two CIDEA linker deletion mutants displayed smaller LD sizes (Fig. S1, *C* and *D*). These results indicate that CIDEC linker (aa 120–135) deletion is unique in enlarging LD sizes.

The enhanced performance of CIDEC(Δ120–135)–GFP in LD fusion and growth may result from one of the two possible reasons, namely close proximity between CIDE-N and CIDE-C domains and removal of inhibitory amino acids. To examine the two possibilities, two deletion CIDEC constructs, namely CIDEC(Δ120–126)–GFP and CIDEC(Δ127–135)–GFP, were constructed. The rationale of these additional constructs is as such: if shortening the distance between CIDE-N and CIDE-C enhances the LD fusion activity, then expressing CIDEC(Δ120–135) with a 16-aa deletion in cells will result in the strongest LD size promotion. This should be followed by CIDEC(Δ127–135) with a 9-aa deletion. The least effective construct will be CIDEC(Δ120–126) with a 7-aa deletion. However, in the various assays, CIDEC(Δ120–126)–GFP expression resulted in the same phenotype as the 16-aa deletion with an increase in the number of supersized LDs in the cells (Fig. S1, *E* and *F*) upon protein normalization (see Fig. S1*H*). CIDEC(Δ127–135)–GFP had little effect on the promotion of LD size. These data indicate that reducing the distance between the CIDE-N and CIDE-C is not the reason for the enhanced LD fusion. Next, in contrast to CIDEC(Δ127–135)–GFP, CIDEC(Δ120–135)–GFP and CIDEC(Δ120–126)–GFP expressions exhibited fewer LDs due to increased LD fusion (Fig. S1*G*). Thus, the results reveal that aa 120–126 are likely to be the key residues in CIDEC responsible for LD size regulation.

Figure 1. Linker region of CIDEC is an inhibitory domain for LD fusion and growth. *A,* schematic diagram showing the 239-amino acid (aa) sequence of murine full-length CIDEC. CIDEC consists of CIDE-N domain (aa 39–119), CIDE-C domain (aa 136–239), and a linker region (aa 120–135). *B,* representative fluorescent images of LDs in 3T3-L1 pre-adipocytes expressing GFP, full-length CIDEC–GFP, and CIDEC(Δ120–135)–GFP as indicated. *Arrowheads,* LDCS. *C,* cell lysates harvested from *B* were separated on SDS-PAGE, and Western blotting was performed with the indicated antibodies. *IB,* immunoblotting. *D,* diameter of the largest LD in each 3T3-L1 pre-adipocyte expressing GFP ($n = 122$), full-length CIDEC–GFP ($n = 91$), and CIDEC(Δ120–135)–GFP ($n = 105$) was measured. *E,* LDs in 3T3-L1 pre-adipocytes expressing the indicated CIDEC constructs corresponding to *D* were classified based on their sizes (0–2, 2–4, and >4 μm) and expressed as percentage to total measured LDs. *F,* number of LDs in each 3T3-L1 pre-adipocyte expressing GFP ($n = 63$), full-length CIDEC–GFP ($n = 86$), and CIDEC(Δ120–135)–GFP ($n = 112$) was counted. *G, upper inset,* representative FRAP images of LD pairs. *Lower inset,* fluorescence recovery percentage of mean of optical intensity (*MOI*) in Bodipy-labeled LDs containing CIDEC(1–239)–GFP and CIDEC(Δ120–135)–GFP at indicated time points. *H,* statistical analysis of neutral lipid-exchange rate between LD pairs in 3T3-L1 pre-adipocytes expressing full-length CIDEC–GFP ($n = 39$) and CIDEC(Δ120–135)–GFP ($n = 32$). *I,* representative time-lapse DIC images of LD pairs. *Arrows,* the acceptor LD, LD_1; *arrowheads,* the donor LD, LD_2. *J,* neutral lipid transfer rate from donor LDs to acceptor LDs in 3T3-L1 pre-adipocytes expressing full-length CIDEC–GFP ($n = 71$) and CIDEC(Δ120–135)–GFP ($n = 76$). ***, $p < 0.001$, calculated using one-way ANOVA with Tukey post hoc test for multiple comparison in *D* and *F*. ***, $p < 0.001$, calculated using a two-tailed Student's *t* test in *H* and *J*. The values are represented as a *box-whisker plot*. *n*, number of cells in *D* and *F* and number of LD pairs in *H* and *J*. *Scale bars,* 20 μm; *insets*: 5 μm in *B*; 2 μm in *G*; and 10 μm in *I*.

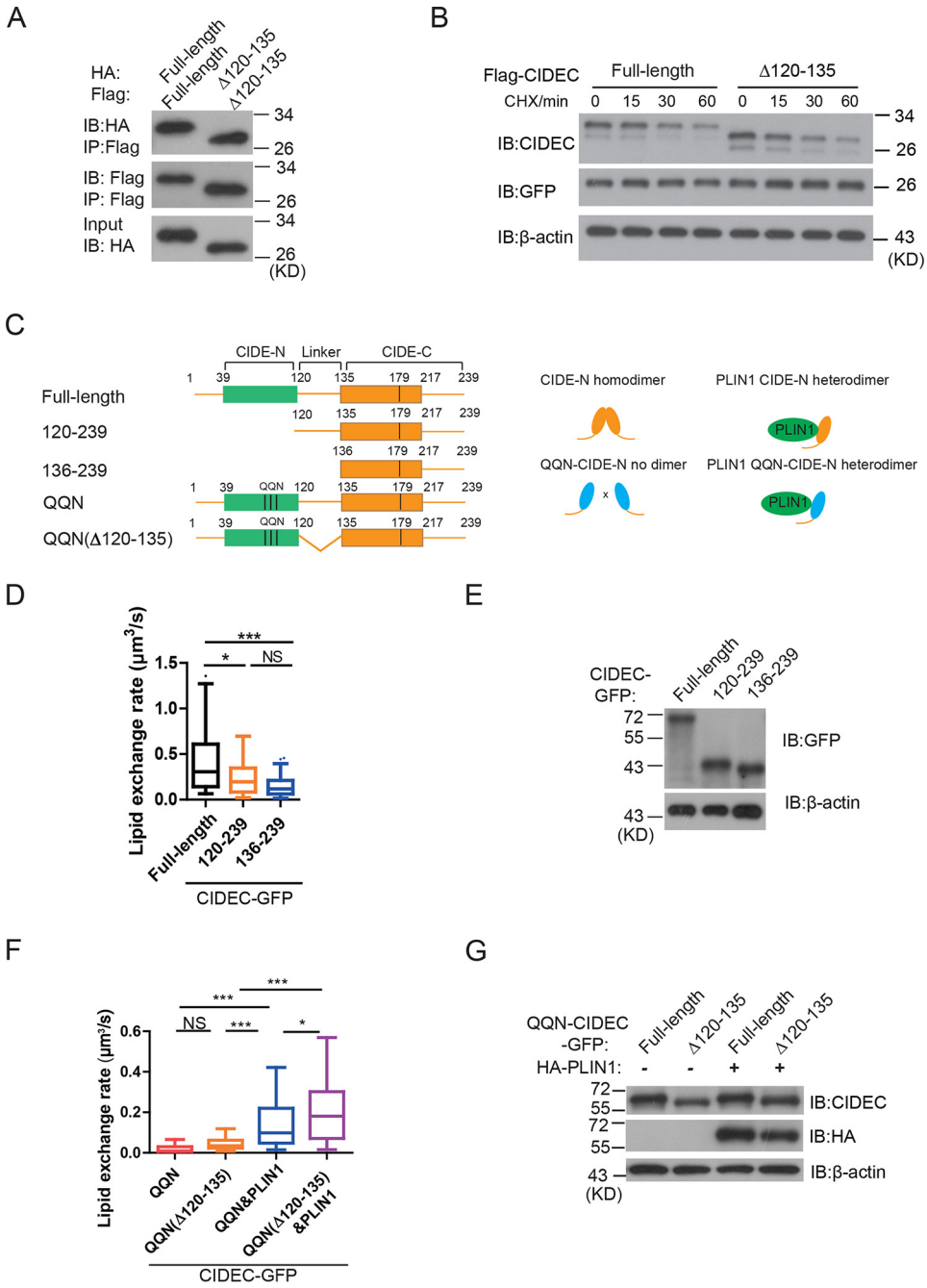

Figure 2. Interaction between CIDE-N domains is required for enhancement of LD fusion via deletion of linker region. *A,* 293T cells were co-transfected with HA full-length CIDEC, FLAG full-length CIDEC, or with HA-CIDEC(Δ120–135) and FLAG-CIDEC(Δ120–135). Cell lysates harvested were immunoprecipitated, and Western blotting was performed with the indicated antibodies. *IB,* immunoblotting; *IP,* immunoprecipitation. *B,* cycloheximide time-chase experiment was performed on 293T cells expressing FLAG full-length CIDEC and FLAG-CIDEC(Δ120–135). Cell lysates were harvested at indicated time points and separated on SDS-PAGE. Western blotting was performed with the indicated antibodies. *C,* schematic diagrams showing the various CIDEC truncations and the interaction between CIDE-N and CIDE-N or between PLIN1 and CIDE-N. *D,* neutral lipid-exchange rates between LD pairs in 3T3-L1 pre-adipocytes expressing full-length CIDEC–GFP ($n = 41$), CIDEC(120–239)–GFP ($n = 32$), and CIDEC(136–239)–GFP ($n = 40$) were measured. *E,* cell lysates harvested from *D* were separated on SDS-PAGE, and Western blotting was performed with the indicated antibodies. *F,* neutral lipid-exchange rates between LD pairs in 3T3-L1 pre-adipocytes expressing QQN-CIDEC–GFP ($n = 28$) and QQN-CIDEC(Δ120–135)–GFP ($n = 49$), co-expressing QQN-CIDEC–GFP with HA-PLIN1 ($n = 32$), and co-expressing QQN-CIDEC(Δ120–135)–GFP with HA-PLIN1 ($n = 42$) were measured. *G,* Western blotting showing the protein expression of the indicated proteins from cells harvested in *F*. *, $p < 0.05$; ***, $p < 0.001$, and *NS,* $p > 0.05$, calculated using one-way ANOVA with Tukey post hoc test for multiple comparison in *D* and *F*. The values are represented as a *box-whisker plot*. *n*, number of LD pairs in *D* and *F*.

Next, to further dissect for the key residue, we substituted CIDEC aa 121–134 with the exception of aa 127, 129, and 133 with alanine and measured the LD sizes when overexpressed in 3T3-L1 pre-adipocytes. The result is summarized in Fig. 3*A*. Interestingly, we found that single mutation of any of the RKKR residues (RKKR/A) within aa 123–126 led to a comparable ability to promote LD growth and increase in the proportion of supersized LDs as CIDEC(Δ120–135) (Fig. 3, *B* and *C*). The phenotypes caused by the point mutations of two residues, K125A and R126A, appeared to be similar to CIDEC(Δ120–

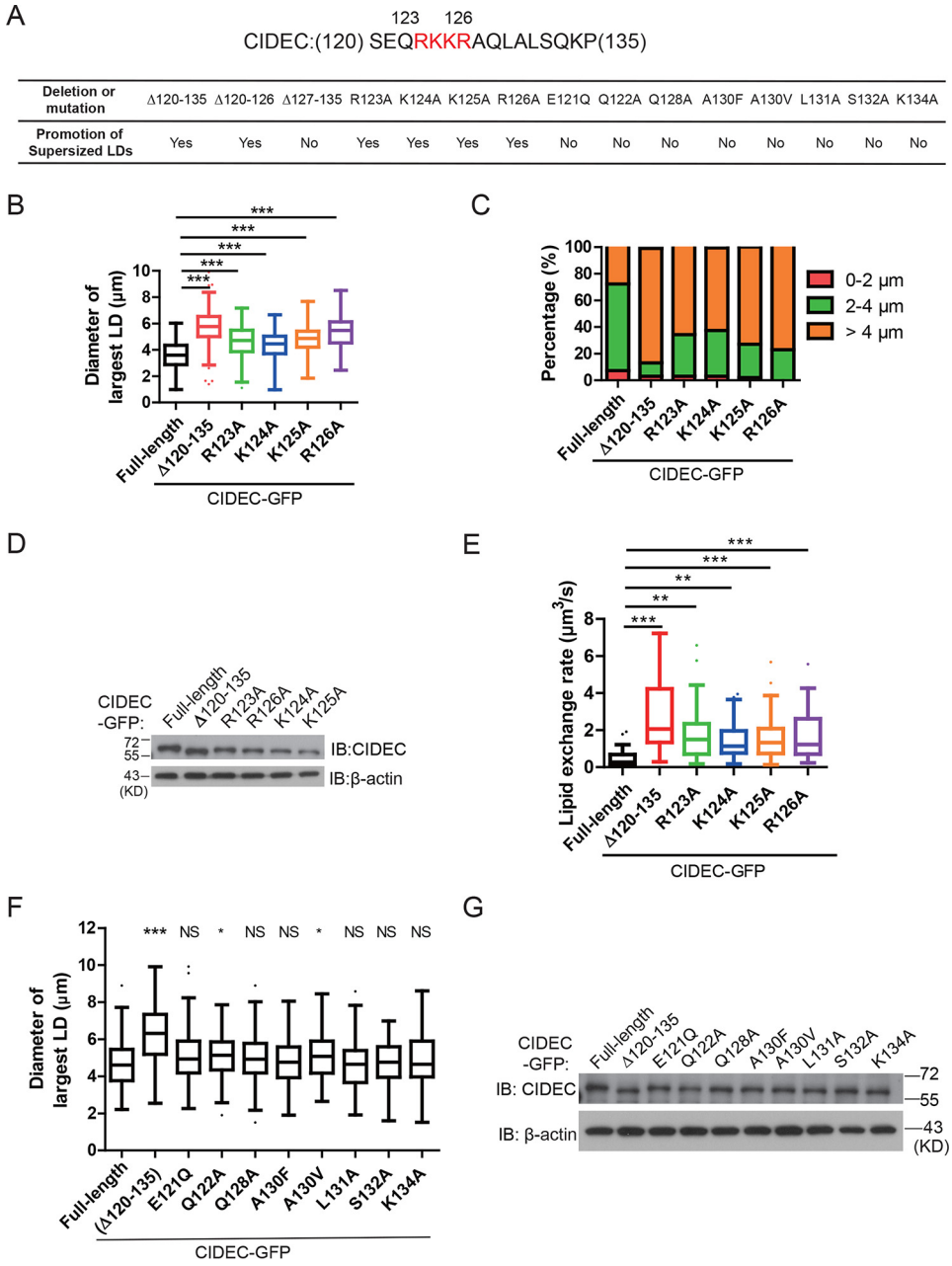

Figure 3. Polybasic RKKR motif restricts enhanced LD fusion ability. *A, upper schematic diagram* shows amino acid sequence 120–135 in murine CIDEC. *Lower table* shows the promoted effect of supersized LD formation induced by CIDEC deletions and mutations. *B,* diameter of the largest LD in each 3T3-L1 pre-adipocyte expressing WT full-length CIDEC–GFP ($n = 124$), CIDEC(Δ120–135)–GFP ($n = 115$), R123A-CIDEC–GFP ($n = 141$), K124A-CIDEC–GFP ($n = 134$), K125A-CIDEC–GFP ($n = 133$), and R126A-CIDEC–GFP ($n = 137$) was measured. *C,* LDs in 3T3-L1 pre-adipocytes expressing the indicated CIDEC constructs corresponding to *B* were classified based on their sizes (0–2, 2–4, and >4 μm) and expressed as percentage to total measured LDs. *D,* cell lysates harvested from *B* were separated on SDS-PAGE, and Western blotting was performed with the indicated antibodies. *IB,* immunoblotting. *E,* neutral lipid-exchange rates between LD pairs in 3T3-L1 pre-adipocytes expressing WT full-length CIDEC–GFP ($n = 35$), CIDEC(Δ120–135)–GFP ($n = 32$), R123A-CIDEC–GFP ($n = 61$), K124A-CIDEC–GFP ($n = 60$), K125A-CIDEC–GFP ($n = 59$), and R126A-CIDEC–GFP ($n = 23$) were measured. *F,* diameter of the largest LD in each 3T3-L1 pre-adipocyte expressing full-length CIDEC–GFP ($n = 126$), CIDEC(Δ120–135)–GFP ($n = 133$), and eight mutants was measured. These mutants were E121Q-CIDEC–GFP ($n = 126$), Q122A-CIDEC–GFP ($n = 129$), Q128A-CIDEC–GFP ($n = 129$), A130F-CIDEC–GFP ($n = 134$), A130V-CIDEC–GFP ($n = 128$), L131A-CIDEC–GFP ($n = 126$), S132A-CIDEC–GFP ($n = 130$), and K134A-CIDEC–GFP ($n = 135$). *G,* protein expression of the 10 CIDEC constructs collected from cells in *F* was determined with Western blotting. *, $p < 0.05$; **, $p < 0.01$; ***, $p < 0.001$, and *NS*, $p > 0.05$, calculated using one-way ANOVA with Tukey post hoc test for multiple comparisons in *B, E,* and *F*. The values are represented as a *box-whisker plot*. *n*, number of cells in *B* and *F* and number of LD pairs in *E*.

135). Western blotting indicated the enhanced effect was not due to the differences in protein expression level (Fig. 3*D*). In addition, similar to the deletion of the linker (aa 120–135), the mutation RKKR/A could individually enhance the lipid-exchange rates between the LD pairs, which were faster than that for full-length CIDEC–GFP (0.44 $\mu m^3/s$ for full-length CIDEC, 1.72 $\mu m^3/s$ for R123A, 1.43 $\mu m^3/s$ for K124A, 1.62 $\mu m^3/s$ for K125A, and 1.80 $\mu m^3/s$ for R126A; Fig. 3*E*). Conversely, other point mutations did not induce the formation of supersized LDs (see Fig. 3, *A*, *F*, and *G*). The results show that the RKKR motif in the linker region of CIDEC is the key sequence that restricted LD fusion and the formation of supersized LDs.

To examine whether the inhibitory function of murine CIDEC linker region is conserved in human CIDEC, we deleted aa 120–134 of human CIDEC corresponding to the murine CIDEC linker region and compared the lipid-exchange rates of these three constructs when expressed in 3T3-L1 pre-adipocytes (Fig. S2, *A* and *B*). The data showed that there was no difference in activities between human and murine CIDEC, and there was no significant difference between full-length and Δ120–134 human CIDEC. These results indicate that the human CIDEC linker region has no inhibitory function as a murine CIDEC. Next, to confirm the difference in function between the human and murine CIDEC linker regions, Arg-125 of human CIDEC was mutated to either Ala (R125A) or Gln (R125Q) and expressed in 3T3-L1 pre-adipocytes. The lipid-exchange rates were measured and compared with murine CIDEC R126A and R126Q mutants. Consistently, murine CIDEC R126A and R126Q enhanced the lipid-exchange rate significantly. This was, however, not observed when human CIDEC R125A/R125Q mutations were expressed (Fig. S2, *C* and *D*). The data further ascertain that the human CIDEC linker region has no role in the regulation of fusion activity. Taken together, the unique inhibitory function of the RKKR motif in the regulation of LD fusion is specific to murine CIDEC protein.

Polybasic RKKR motif interacts with acidic phospholipids

The gain-of-function for LD fusion by the deletion or mutation of CIDEC is intriguing. Some researchers reported that polybasic residue clusters composed of lysine and arginine are inclined to interact with acidic phospholipids (46–49). This kind of electrostatic attraction is important physiologically, thus enabling protein binding to membrane, protein enrichment, and protein–protein interaction (46–49). For cellular LDs, the composition of the phospholipid monolayer depends on the cell type but mostly consists of neutral phospholipids PC, PE, and acidic phospholipids that possess negatively charged polar heads. These include PS, PA, and PI (50). Here, we hypothesized that CIDEC interacts with the phospholipids via the polybasic RKKR motif. We adopted an aromatic fluorescence emission assay to detect the interaction between the peptides and phospholipids (Fig. 4*A*). When peptides with aromatic amino acids were attached to a liposome composed of phospholipids, there was a decrease in their movement in the solution. This was followed by an increase in emission intensity, which can be captured in the presence of an excitation light of wavelength 280 nm. Here, WT peptide and the RKKR mutant (4A) peptide, both with a tryptophan, were synthesized and used in a tryptophan fluorescence emission assay (Fig. 4*A*). The calculation of their net charge shows that the WT peptide is positively charged, whereas the mutated RKKR to alanine reduces positive charges (Fig. 4*A*). Assay data show that the WT peptides displayed increased association with PS, PA, and PI in a dose-dependent manner (Fig. 4, *B–D*). Interestingly, the WT peptides had a lower saturation concentration of 20 μM when incubated with PA liposomes compared with PS and PI liposomes, indicating stronger interaction with PA. It is noted here that the WT peptide was unable to interact with PC liposomes (Fig. 4*E*). The results show that the WT peptide can specifically bind to acidic phospholipids, especially PA. By contrast, the 4A peptides completely lost the ability to bind to PS, PA, PI, or PC liposomes (Fig. 4, *F–I*) with unchanged emission intensity in the presence of different concentrations of phospholipids. The data imply that the loss of the RKKR motif disrupted their electrostatic interaction with the acidic phospholipids. In addition, binding to acidic phospholipids by the control peptide with alanine replacement on Lys-134 (K134A) remained unaffected (Fig. S3, *A–C*). The results are summarized in table format in Fig. 4*J*. Next, we ask whether all four polybasic residues were required for the interaction with PA. Here, three additional mutant peptides with single, double, or triple basic amino acid replacements were constructed. They are K125A (1A), K125A/R126A (2A), and K124A/K125A/R126A (3A). Using these peptides, tryptophan fluorescence emission experiments were performed and compared with WT and 4A peptides (Fig. 4*K*). The results showed that the binding activities of these mutant peptides reduced progressively with each successive point mutations to alanine. The ranking of binding activities is as follows: (strongest) WT > K125A > 2A > 3A > 4A (weakest). In other words, the K125A mutant had a weaker binding ability than the WT linker region of CIDEC. These data indicate that with more elimination of the positive charge amino acid on the polybasic motif, concomitantly, the binding activity of the peptide to PA was reduced. These data indicate that the CIDEC–lipid interaction depends on the number of polybasic residues. Every positive charge loss will gradually reduce the binding activity of the peptide to PA.

Circular dichroism assay was commonly used to survey the peptide–lipid interaction. The PA molecule was reported to play an important role in CIDEA-mediated LD fusion (39). Here, we analyzed the CD spectra of both WT and 4A mutant peptides in aqueous solution or with PC or PA liposomes. The results revealed that WT or 4A mutant peptides were unordered in buffer solution and in the presence of PC liposomes. However, in the presence of PA liposomes, both peptides exhibited α-helix conformation (Fig. S3, *D* and *E*). Furthermore, the conformational change to α-helix for WT peptide was relatively higher compared with 4A mutant peptides, indicating the presence of a stronger interaction between the WT peptide and PA phospholipid. The loss of polybasic residues resulted in much weaker interaction between peptide and phospholipid. Here, it is revealed that the polybasic RKKR motif on CIDEC preferably binds to the acidic phospholipids by means of electrostatic interaction.

Loss of polybasic RKKR motif promotes CIDEC-mediated LD fusion and growth

Finally, to further demonstrate the positively charged RKKR motif indeed has an effect on the LD size regulation, we replaced the RKKR with glutamine. Glutamine is similar in size to arginine and lysine but is electrically neutral (Fig. 5*A*). Expectantly, the RKKR/Q mutants behaved similarly to aa 120–126 deletion, inducing the formation of supersized LDs when overexpressed (Fig. 5, *B–D*). These data indicate that the gain-of-function by the mutant was mainly due to the change in the charge property of the residues instead of their size. This is further corroborated; aa 123–126 (RKKR) were individually

A

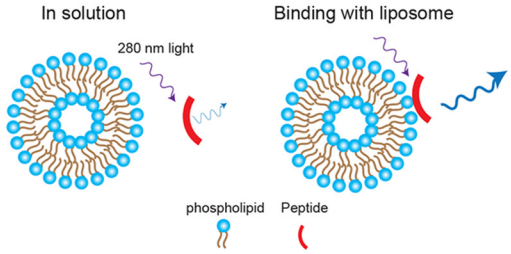

	Sequence	pI	Net charge
WT	KWKPPSEQRKKRAQLALSQKP	10.22	+ 6.0
4A	KWKPPSEQAAAAAQLALSQKP	9.70	+ 2.0

B

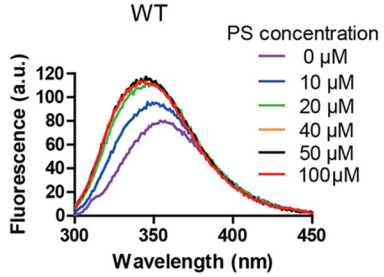

F

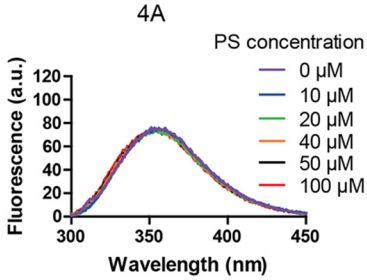

C

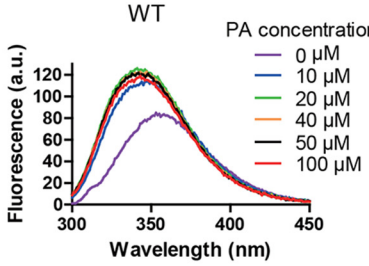

G

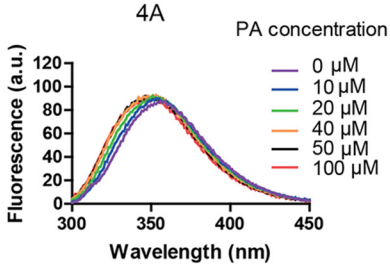

D

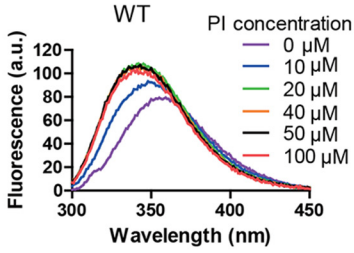

H

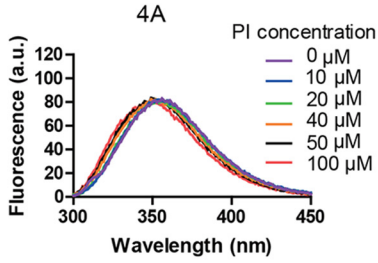

E

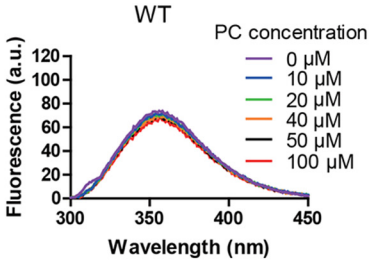

I

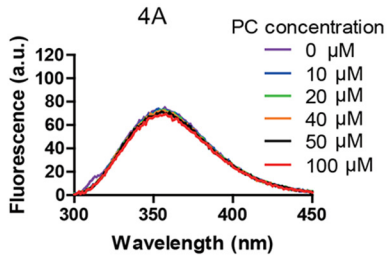

J

Peptide	Binding with phospholipids			
	PS	PA	PI	PC
WT	Yes	Yes	Yes	No
4A	No	No	No	No

K

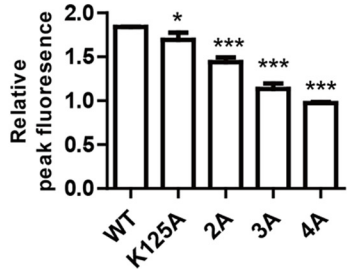

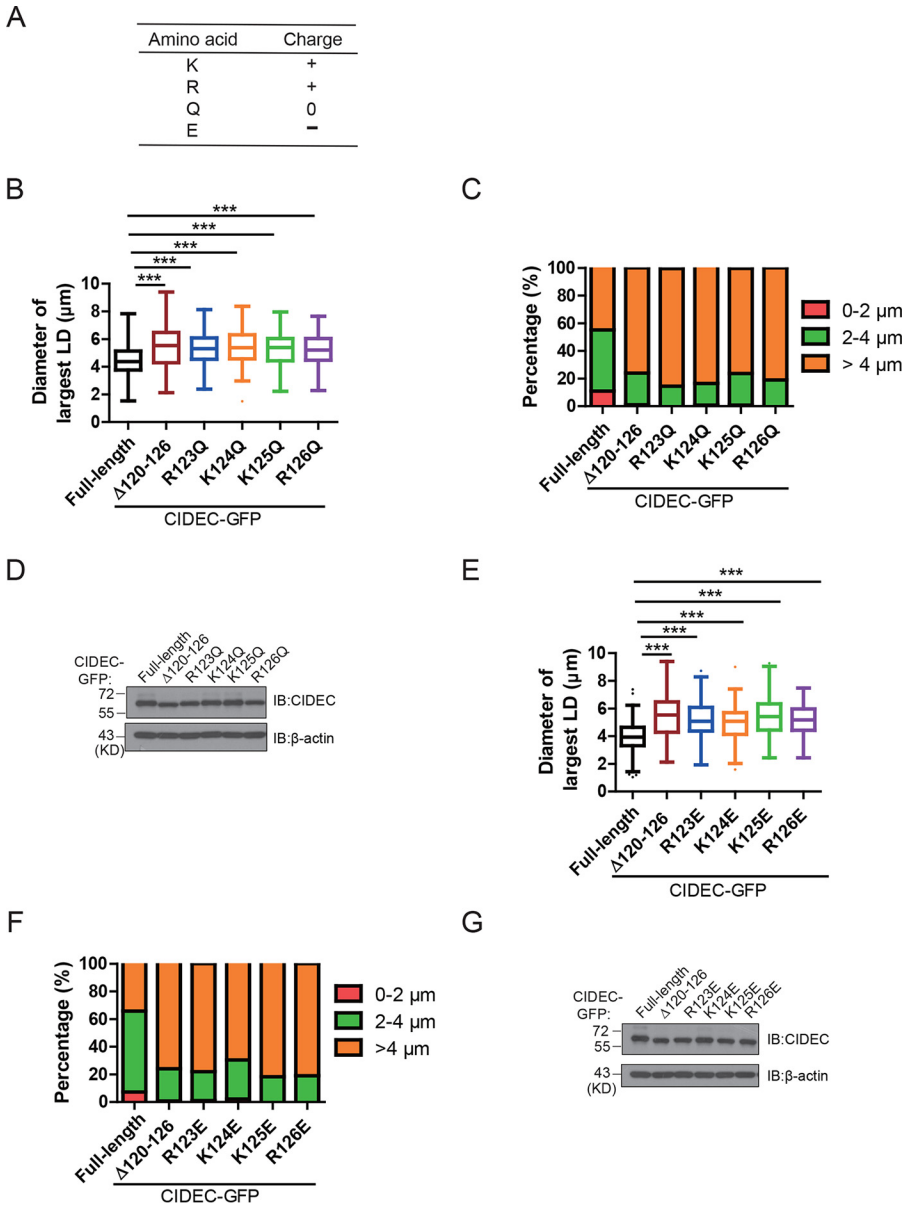

Figure 5. Charge replacements of RKKR amino acids lead to enhanced growth of LDs. *A, table* showing the differences in charge of amino acid among lysine (*K*), arginine (*R*), glutamine (*Q*), and glutamic acid (*E*). *B,* diameter of the largest LD in each 3T3-L1 pre-adipocyte expressing WT full-length CIDEC–GFP ($n = 138$), CIDEC(Δ120–126)–GFP ($n = 133$), R123Q-CIDEC–GFP ($n = 138$), K124Q-CIDEC–GFP ($n = 128$), K125Q-CIDEC–GFP ($n = 140$), or R126Q-CIDEC–GFP ($n = 148$) was measured. *C,* LDs in 3T3-L1 pre-adipocytes expressing the indicated CIDEC constructs corresponding to *B* were classified based on their sizes (0–2, 2–4, and >4 μm) and expressed as percentage to total measured LDs. *D,* cell lysates harvested from *B* were separated on SDS-PAGE, and Western blotting was performed with the indicated antibodies. *IB,* immunoblotting. *E,* diameter of the largest LD in each 3T3-L1 pre-adipocyte expressing full-length CIDEC–GFP ($n = 138$), CIDEC(Δ120–126)–GFP ($n = 133$), R123E-CIDEC–GFP ($n = 140$), K124E-CIDEC–GFP ($n = 138$), K125E-CIDEC–GFP ($n = 137$), or R126E-CIDEC–GFP ($n = 148$) was measured. *F,* LDs in 3T3-L1 pre-adipocytes expressing the indicated CIDEC constructs corresponding to *E* were classified based on their sizes (0–2, 2–4, and >4 μm) and expressed as percentage to total measured LDs. *G,* cell lysates harvested from *E* were separated on SDS-PAGE, and Western blotting was performed with the indicated antibodies. ***, $p < 0.001$, calculated using one-way ANOVA with Tukey post hoc test for multiple comparison in *B* and *E*. The values are represented as a *box-whisker plot*. *n*, number of cells in *B* and *E*.

Figure 4. Polybasic RKKR motif interacts with acidic phospholipids. *A, left,* schematic diagram of the tryptophan fluorescence emission assay used to measure the binding of peptides to phospholipids. *Right,* amino acid sequences and charge properties of wildtype (*WT*) and mutant RKKR/A (*4A*) peptides used in tryptophan fluorescence emission experiments. *B–E,* tryptophan fluorescence emission assay was used to measure the binding of WT peptide to liposomes individually composed of PS (*B*), PA (*C*), PI (*D*), or PC (*E*) at various specified concentrations. Data shown are representative of three independent experiments. *F–I,* binding of 4A peptide to liposomes composed of PS (*F*), PA (*G*), PI (*H*), or PC (*I*) at various specified concentrations was determined using the tryptophan fluorescence emission assay. Data shown are representative of three independent experiments. *J, summary table* showing the interaction between WT and 4A peptide with PS, PA, PI, and PC. *K,* relative peak fluorescence fold change of WT, K125A, K125A/R126A (*2A*), K124A/K125A/R126A (*3A*), and 4A peptides in PA liposomes binding assay. Data shown were the average of three independent experiments. *, $p < 0.05$, and ***, $p < 0.001$, calculated using one-way ANOVA with Tukey post hoc test for multiple comparison in *K*.

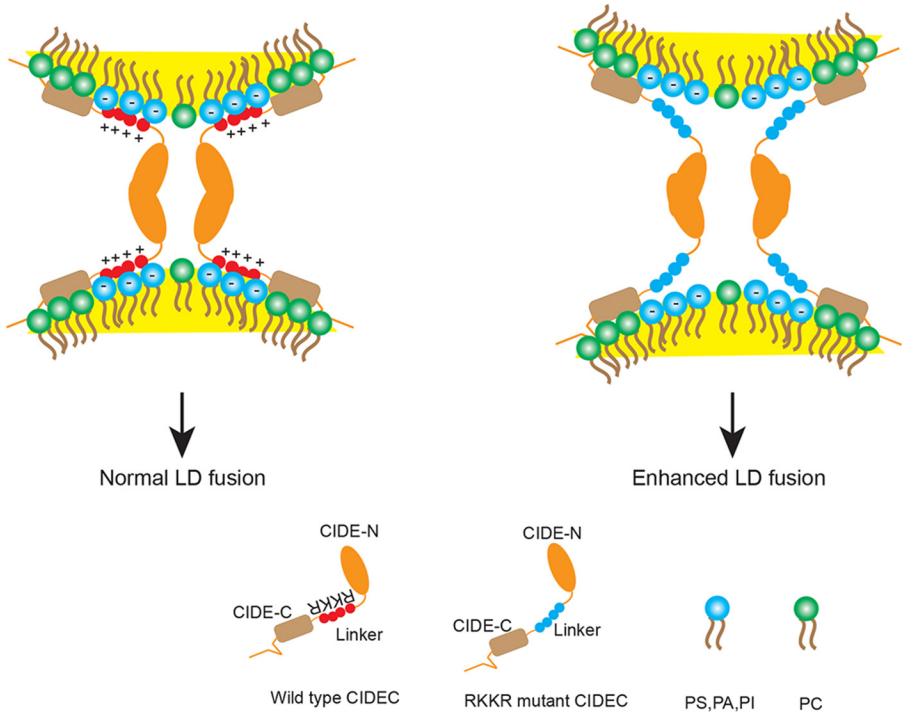

Figure 6. Model for the function of CIDEC RKKR motif in regulating LD fusion and growth. RKKR motif in the linker region of CIDEC interacts with the acidic phospholipids of the LD monolayer. When this motif is deleted or replaced, the electrical interaction between the protein and phospholipids is lost. This results in greater structural flexibility for the mutant proteins and enables the formation of larger fusion pores which in turn promotes LD fusion and growth.

replaced with negatively charged glutamic acid. The results show that the RKKR/E expression displayed a similarly enhanced LD fusion and growth effect to that of CIDEC(Δ120–126) (Fig. 5, *E–G*). Taken together, these data confirm that the promotion of supersized LD formation via LD fusion was primarily due to the loss of the polybasic RKKR motif.

Discussion

In this work, we first identify a unique regulation by aa 120–135 in CIDEC-mediated LD fusion. Deletion of the linker promotes the formation of supersized LDs. This enhanced LD fusion phenotype is the result of increased lipid exchange and lipid transfer rates. The formation of supersized LDs requires the interaction between CIDE-N domains and works differently from PLIN1. Importantly, this regulation is determined by the polybasic RKKR motif in the linker. These data provide new insight into the regulation of CIDEC-mediated LD fusion through electrostatic interaction between the RKKR motif and the acidic phospholipids on the LD surface.

Our long-standing interest on the CIDE proteins mediating LD fusion drives this work to further dissect the CIDEC molecule and the function of its domains. Previously, our group reported that the CIDE-C domain possesses the ability to mediate LD fusion albeit with lower activity (16). The CIDE-N domain possesses a conserved Lys-56 acetylation site, which is important for its protein stability and fusion activity (51). Recently, two types of protein structures were found to associate with LD, amphipathic α-helices and hydrophobic hairpins (50). Interestingly, the CIDE-C domain of CIDEC also contains amphipathic α-helices and hydrophobic regions (16), in which the positively charged KKR amino acids play a critical role in CIDEC-mediated LD fusion (16, 20). Furthermore, it was reported that the interaction of the CIDE-C domain with PA might be necessary for LD fusion (39). Thus, we propose that the polybasic motif, including lysine and arginine on CIDEC, is a crucial regulator for LD fusion activity. This type of polybasic motif–phospholipid interaction is commonly found in the biological system. Well-known examples include some small GTPases (Ras, Rab, Arf, and Rho proteins) with polybasic clusters being targeted to the plasma membrane through interaction with phospholipids such as phosphatidylinositol 3,4,5-trisphosphate and phosphatidylinositol 4,5-bisphosphate (52). The polybasic domain was also reported to regulate the phosphorylation of Lipin1 (53). Separately, a polybasic KKR motif in NiV-F protein modulates cell–cell fusion (54). The polybasic region of Rac1 was proven to interact with the effector protein PRK1 (55). In our study, we confirmed that the polybasic RKKR motif in the linker region of CIDEC interacts with the acidic phospholipids on the LD monolayer. Interestingly, double mutations of the RKKR motif had a similar effect as the single mutation to promote the formation of supersized LDs (data not shown). We speculate that any change to the RKKR motif is sufficient to induce conformational change on CIDEC, making it difficult to interact with the phospholipids on the highly curved LD surface.

Based on the above observations, we propose a model to interpret the effect of the polybasic RKKR motif on CIDEC during LD fusion (Fig. 6). CIDEC comprises three domains: CIDE-N domain, CIDE-C domain, and the linker region. When two LDs are in close range, the CIDE-N domains of the CIDEC molecules homodimerize at LDCS, facilitating local enrichment of the CIDEC proteins. The RKKR motif in the linker region interacts with the acidic phospholipids of the LD mono-

layer through electrostatic attraction. With these, the conformational freedom of the CIDE-N domain is further restricted by the CIDEC–phospholipid interaction and enables the assembly of protein complexes at the LDCS for the formation of fusion pore, allowing neutral lipid exchange. The internal pressure difference derived from LD surface tension leads to lipid transfer from the donor to the acceptor LD. When the polybasic RKKR motif is mutated or deleted, the interaction of the linker region with acidic phospholipids is disrupted, and CIDEC proteins are unrestrained, achieving conformational freedom between the CIDE-N and CIDE-C domains. With the CIDE-N dimerization holding the CIDEC proteins in place, the newly formed fusion pore at the LDCS is enlarged and leads to enhanced LD fusion and supersized LD.

This investigation provides insight into CIDEC's role in LD fusion and growth. However, the regulatory role of the RKKR motif *in vivo* remains to be determined. In addition, future works are required to determine whether the motif directly influences the fusion pore size and whether the motif works collaboratively with the two CIDE-domains. In summary, more detailed studies are needed to uncover the relationship of the CIDEC–lipid interaction with the enhanced LD fusion ability.

Experimental procedures

Reagents and antibodies

M2 beads and sodium oleate (OA) were purchased from Sigma. WT and mutant CIDEC peptides were synthesized at GenScript. Phospholipids were purchased from Avanti Polar Lipid. Bodipy C12 was purchased from ThermoFisher Scientific. The antibody against CIDEC was used as described previously (16, 17). Antibodies against β-actin (mouse, A5441) and FLAG (mouse, F1804) were purchased from Sigma. Antibodies against GFP (rabbit, sc-8334) and HA (mouse, sc-7392) were purchased from Santa Cruz Biotechnology.

Plasmid DNA construction

Full-length cDNAs encoding CIDEC, CIDEA, and PLIN1 were amplified from cDNA of mouse adipose tissue and cloned into pEGFPN1, pCMV5-HA, or pCMV5-FLAG vectors. Deletion fragments of CIDEC and CIDEA were amplified from full-length CIDEC or CIDEA by appropriate primers. Full-length cDNA encoding human CIDEC was amplified from cDNA of human adipose tissue and cloned into the pEGFPN1 vector. The deletions were subcloned into XhoI–EcoRI sites of pEGFPN1 or NdeI–BamHI sites of pCMV5-HA and pCMV5-FLAG vectors. Point mutations of CIDEC were generated using PCR site-directed mutagenesis from full-length CIDEC. All plasmid DNA constructs were sequenced to guarantee the fidelity.

Cell culture

293T cells and 3T3-L1 pre-adipocytes were cultured in Dulbecco's modified Eagle's medium supplemented with 10% fetal bovine serum (Gibco), 2 mM L-glutamine, 100 μg/ml streptomycin, and 100 units/ml penicillin. Cells were grown at 37 °C in a humidified incubator containing 5% CO_2. Plasmid DNAs were transfected into 293T cells using polyethyleneimine solution (Polyscience) according to the manufacturer's instruction. Electroporation of plasmid DNA into 3T3-L1 pre-adipocytes was done by using Amaxa Nucleofector II (Lonza) with program A-033.

Fluorescence imaging

Cells were transfected with the indicated GFP vectors and grown on a coverslip. Subsequently, the coverslips of cells were immersed in medium supplemented with 1 μg/ml Bodipy 558/568 C12 fatty acid (Molecular Probes) and 200 μM OA for 20–24 h. Cells were washed twice with PBS, fixed with 4% paraformaldehyde, followed by incubation with Hoechst in PBS. For fixed cells, images were collected using a Nikon A1R+ confocal microscope with a $\times$100 oil-immersion objective and three lasers (405/488/561 nm in wavelength). For z-stack images, images with a step interval of 0.2 μm were acquired. Live cell imaging was performed as described previously (17).

Size measurement of lipid droplets

Cells with GFP fluorescent signals were randomly selected from transfected cells. Images were taken using a Carl Zeiss inverted microscope (Axiovert 200M) with a $\times$63 oil-immersion objective. The diameter of a largest LD in each cell was measured by using ImageJ software. The sizes of largest LDs were analyzed and plotted using GraphPad Prism 5.

Lipid-exchange rate assay

Lipid-exchange rate assay was performed as described previously (17) with some modifications. 3T3-L1 pre-adipocytes were transfected with the indicated plasmids (CIDEC and PLIN1) and were incubated with 200 μM OA and 1 μg/ml Bodipy 558/568 C12 fatty acid (Molecular Probes) for 18 h. Cells were transferred to fresh medium 1 h before FRAP experiments. Cells were cultured in a living cell station (Oko laboratory) and viewed under a confocal microscope (A1Rsi, Nikon) using a $\times$100 oil-immersion objective. Digital detector gain and laser power were set to avoid overexposure and to ensure accurate quantification of fluorescence. The bleaching area of a LD was set to ensure that at least 70% of its total area was covered and bleached by 120 ms at 100% laser power of a 561-nm solid-state laser. This was followed by time-lapse scanning of 50 frames with an interval of 1.12 s. The bleaching process was performed on the smaller LD three times for statistical analyses. As there are more fluorescent molecules in the larger LD of the LD pair, bleaching these large LDs more than twice will result in enormous reduction in fluorescent intensity. This in turn may cause the fluorescent intensities within the cores of the LD pair to decline rapidly and pose difficulty in the detection of the fluorescence recovery. Mean optical intensities within the LD core regions were measured simultaneously. A set of LD pairs was analyzed in each experiment, and unbefitting data were filtered out based on the criteria in the exchange-rate assay.

Lipid transfer rate assay

Live cells overexpressed with the indicated CIDEC–GFP plasmid were incubated on a living cell station (Oko laboratory). Differential interference contrast (DIC) images were acquired using a Nikon A1R+ confocal microscope with a

×100 oil-immersion objective. Time-lapse images were taken with an interval of 2 min for at least 4 h.

Image processing and analysis

Images were processed using NIS-element analysis (Nikon) or ImageJ. Cropping of images was done using Photoshop 5 (Adobe). The LD number per cell was determined using Imaris 9 (Bitplane) with a spot mode. The LD volume per cell was measured using NIS-element software (Nikon).

Protein stability assay

The stability of CIDEC proteins was analyzed based on CHX protein-chase experiment as described previously (56). 293T cells were transfected with FLAG-tagged full-length CIDEC or its deletion. Twenty hours after transfection, the medium was replaced with fresh medium supplemented with CHX (100 μg/ml). Cells were harvested at the indicated time points (0, 15, 30, and 60 min).

Immunoprecipitation

293T cells were transfected with HA- and FLAG-tagged CIDEC plasmids and cultured in an incubator for 20–24 h. Cells were lysed with IP buffer (20 mM HEPES, 150 mM NaCl, 1% EDTA, 1% EGTA, 1% Trion X-100, 1% phenylmethylsulfonyl fluoride) and centrifuged to remove nuclei. The supernatant was incubated with M2 beads (Sigma) for 2–3 h followed by three washes. The M2 beads were added with loading buffer and separated on SDS-PAGE.

Liposome preparation

1 ml of liposome stock consisting of 5 mM of the indicated phospholipid was prepared by dissolving appropriate weight of lipids according to their molecular weight in 1 ml of chloroform. The lipid/chloroform solution was dried under vacuum by rotary evaporation to form a homogeneous lipid layer. The lipid thin film was dissolved in 1 ml of distilled water, frozen, and thawed for five times with liquid nitrogen to form large unilamellar vesicles (LUVs). The LUVs were homogenized with an extruder through a 0.1-μm filter (Whatman) 15 times to form liposomes.

Tryptophan fluorescence emission

WT and mutation peptides composed of CIDEC aa 115–135 at a final concentration of 2 μM were incubated with liposomes, which comprise electroneutral phospholipids or acidic phospholipids, in Tris-HCl buffer (100 mM, pH 7.4) at room temperature for 5 min and then detected on a Varian Cary Eclipse machine. The concentrations of phospholipids in the form of liposomes were 10, 20, 40, 50, and 100 μM, respectively. The excitation wavelength was 280 nm, and the scanning wavelength of emission light was set at 300–450 nm to cover the emission peak. The spectra were acquired with a scan rate of 120 nm/min, a data interval of 1 nm, and a photomultiplier tube voltage of medium. The results were analyzed by subtraction of the appropriate buffer or liposome fluorescence spectrum.

CD

Circular dichroism (CD) experiments were performed using a Jasco J-715 spectrometer (Jasco, UK) with indicated peptides (GenScript) at a concentration of 20 μM in 2 mM Tris-HCl, pH 7.4. A 2-mm path-length quartz cuvette (Hellma) was adopted in the experiments. The spectra were recorded between 190 and 250 nm with a data pitch of 0.2 nm, a bandwidth of 2 nm, a scan rate of 200 nm/min, and a response time of 1 s. CD spectra were recorded with peptide samples incubated with or without PC or PA liposomes of 200 μM at 22 °C. Data shown were averaged from three independent spectra after subtraction of the appropriate buffer or liposomes CD spectrum.

Statistics

Statistical analyses of all data were done using GraphPad Prism 5. The two-tailed Student's t test was performed for a single comparison, and the one-way ANOVA with Tukey post hoc test was performed for multiple comparisons. Differences were considered to be significant at $p < 0.05$. p values were indicated in each figure as follows: *, $p < 0.05$; **, $p < 0.01$; ***, $p < 0.001$.

Author contributions—J. W., P. L., and F.-J. C. conceptualization; J. W. and F.-J. C. formal analysis; J. W. investigation; J. W. and F.-J. C. writing-original draft; C. Y. and C. X. resources; C. Y. and C. X. methodology; C. X., P. L., and F.-J. C. supervision; B. T. C. and P. L. writing-review and editing; P. L. funding acquisition; P. L. and F.-J. C. project administration; F.-J. C. visualization.

Acknowledgments—We thank the members of the P. Li Laboratory at Tsinghua University for their helpful discussions and Jinyu Wang at SLSTU-Nikon Biological Imaging Center for imaging supporting.

References

1. Farese, R. V., Jr., and Walther, T. C. (2009) Lipid droplets finally get a little R-E-S-P-E-C-T. *Cell* **139,** 855–860 CrossRef Medline
2. Greenberg, A. S., Coleman, R. A., Kraemer, F. B., McManaman, J. L., Obin, M. S., Puri, V., Yan, Q. W., Miyoshi, H., and Mashek, D. G. (2011) The role of lipid droplets in metabolic disease in rodents and humans. *J. Clin. Invest.* **121,** 2102–2110 CrossRef Medline
3. Gross, D. A., and Silver, D. L. (2014) Cytosolic lipid droplets: from mechanisms of fat storage to disease. *Crit. Rev. Biochem. Mol. Biol.* **49,** 304–326 CrossRef Medline
4. Krahmer, N., Farese, R. V., Jr., and Walther, T. C. (2013) Balancing the fat: lipid droplets and human disease. *EMBO Mol. Med.* **5,** 973–983 CrossRef Medline
5. Xu, L., Zhou, L., and Li, P. (2012) CIDE proteins and lipid metabolism. *Arterioscler. Thromb. Vasc. Biol.* **32,** 1094–1098 CrossRef Medline
6. Liu, L., Zhang, K., Sandoval, H., Yamamoto, S., Jaiswal, M., Sanz, E., Li, Z., Hui, J., Graham, B. H., Quintana, A., and Bellen, H. J. (2015) Glial lipid droplets and ROS induced by mitochondrial defects promote neurodegeneration. *Cell* **160,** 177–190 CrossRef Medline
7. Gong, J., Sun, Z., and Li, P. (2009) CIDE proteins and metabolic disorders. *Curr. Opin. Lipidol.* **20,** 121–126 CrossRef Medline
8. Khandelia, H., Duelund, L., Pakkanen, K. I., and Ipsen, J. H. (2010) Triglyceride blisters in lipid bilayers: implications for lipid droplet biogenesis and the mobile lipid signal in cancer cell membranes. *PLoS ONE* **5,** e12811 CrossRef Medline
9. Zanghellini, J., Wodlei, F., and von Grünberg, H. H. (2010) Phospholipid demixing and the birth of a lipid droplet. *J. Theor. Biol.* **264,** 952–961 CrossRef Medline
10. Gross, D. A., Zhan, C., and Silver, D. L. (2011) Direct binding of triglyceride to fat storage-inducing transmembrane proteins 1 and 2 is important for lipid droplet formation. *Proc. Natl. Acad. Sci. U.S.A.* **108,** 19581–19586 CrossRef Medline

11. Choudhary, V., Ojha, N., Golden, A., and Prinz, W. A. (2015) A conserved family of proteins facilitates nascent lipid droplet budding from the ER. *J. Cell Biol.* **211,** 261–271 CrossRef Medline
12. Fujimoto, Y., Itabe, H., Kinoshita, T., Homma, K. J., Onoduka, J., Mori, M., Yamaguchi, S., Makita, M., Higashi, Y., Yamashita, A., and Takano, T. (2007) Involvement of ACSL in local synthesis of neutral lipids in cytoplasmic lipid droplets in human hepatocyte HuH7. *J. Lipid Res.* **48,** 1280–1292 CrossRef Medline
13. Xu, D., Li, Y., Wu, L., Li, Y., Zhao, D., Yu, J., Huang, T., Ferguson, C., Parton, R. G., Yang, H., and Li, P. (2018) Rab18 promotes lipid droplet (LD) growth by tethering the ER to LDs through SNARE and NRZ interactions. *J. Cell Biol.* **217,** 975–995 CrossRef Medline
14. Jacquier, N., Choudhary, V., Mari, M., Toulmay, A., Reggiori, F., and Schneiter, R. (2011) Lipid droplets are functionally connected to the endoplasmic reticulum in *Saccharomyces cerevisiae*. *J. Cell Sci.* **124,** 2424–2437 CrossRef Medline
15. Ohsaki, Y., Cheng, J., Suzuki, M., Fujita, A., and Fujimoto, T. (2008) Lipid droplets are arrested in the ER membrane by tight binding of lipidated apolipoprotein B-100. *J. Cell Sci.* **121,** 2415–2422 CrossRef Medline
16. Gong, J., Sun, Z., Wu, L., Xu, W., Schieber, N., Xu, D., Shui, G., Yang, H., Parton, R. G., and Li, P. (2011) Fsp27 promotes lipid droplet growth by lipid exchange and transfer at lipid droplet contact sites. *J. Cell Biol.* **195,** 953–963 CrossRef Medline
17. Sun, Z., Gong, J., Wu, H., Xu, W., Wu, L., Xu, D., Gao, J., Wu, J. W., Yang, H., Yang, M., and Li, P. (2013) Perilipin1 promotes unilocular lipid droplet formation through the activation of Fsp27 in adipocytes. *Nat. Commun.* **4,** 1594 CrossRef Medline
18. Wu, L., Xu, D., Zhou, L., Xie, B., Yu, L., Yang, H., Huang, L., Ye, J., Deng, H., Yuan, Y. A., Chen, S., and Li, P. (2014) Rab8a-AS160-MSS4 regulatory circuit controls lipid droplet fusion and growth. *Dev. Cell* **30,** 378–393 CrossRef Medline
19. Inohara, N., Koseki, T., Chen, S., Wu, X., and Núñez, G. (1998) CIDE, a novel family of cell death activators with homology to the 45 kDa subunit of the DNA fragmentation factor. *EMBO J.* **17,** 2526–2533 CrossRef Medline
20. Gao, G., Chen, F. J., Zhou, L., Su, L., Xu, D., Xu, L., and Li, P. (2017) Control of lipid droplet fusion and growth by CIDE family proteins. *Biochim Biophys Acta Mol. Cell Biol. Lipids* **1862,** 1197–1204 CrossRef Medline
21. Zhou, Z., Yon Toh, S., Chen, Z., Guo, K., Ng, C. P., Ponniah, S., Lin, S. C., Hong, W., and Li, P. (2003) Cidea-deficient mice have lean phenotype and are resistant to obesity. *Nat. Genet.* **35,** 49–56 CrossRef Medline
22. Zhou, L., Xu, L., Ye, J., Li, D., Wang, W., Li, X., Wu, L., Wang, H., Guan, F., and Li, P. (2012) Cidea promotes hepatic steatosis by sensing dietary fatty acids. *Hepatology* **56,** 95–107 CrossRef Medline
23. Ye, J., Li, J. Z., Liu, Y., Li, X., Yang, T., Ma, X., Li, Q., Yao, Z., and Li, P. (2009) Cideb, an ER- and lipid droplet-associated protein, mediates VLDL lipidation and maturation by interacting with apolipoprotein B. *Cell Metab.* **9,** 177–190 CrossRef Medline
24. Zhang, L. J., Wang, C., Yuan, Y., Wang, H., Wu, J., Liu, F., Li, L., Gao, X., Zhao, Y. L., Hu, P. Z., Li, P., and Ye, J. (2014) Cideb facilitates the lipidation of chylomicrons in the small intestine. *J. Lipid Res.* **55,** 1279–1287 CrossRef Medline
25. Li, J. Z., Ye, J., Xue, B., Qi, J., Zhang, J., Zhou, Z., Li, Q., Wen, Z., and Li, P. (2007) Cideb regulates diet-induced obesity, liver steatosis, and insulin sensitivity by controlling lipogenesis and fatty acid oxidation. *Diabetes* **56,** 2523–2532 CrossRef Medline
26. Toh, S. Y., Gong, J., Du, G., Li, J. Z., Yang, S., Ye, J., Yao, H., Zhang, Y., Xue, B., Li, Q., Yang, H., Wen, Z., and Li, P. (2008) Up-regulation of mitochondrial activity and acquirement of brown adipose tissue-like property in the white adipose tissue of fsp27 deficient mice. *PLoS ONE* **3,** e2890 CrossRef Medline
27. Nishino, N., Tamori, Y., Tateya, S., Kawaguchi, T., Shibakusa, T., Mizunoya, W., Inoue, K., Kitazawa, R., Kitazawa, S., Matsuki, Y., Hiramatsu, R., Masubuchi, S., Omachi, A., Kimura, K., Saito, M., *et al.* (2008) FSP27 contributes to efficient energy storage in murine white adipocytes by promoting the formation of unilocular lipid droplets. *J. Clin. Invest.* **118,** 2808–2821 Medline
28. Rubio-Cabezas, O., Puri, V., Murano, I., Saudek, V., Semple, R. K., Dash, S., Hyden, C. S., Bottomley, W., Vigouroux, C., Magré, J., Raymond-Barker, P., Murgatroyd, P. R., Chawla, A., Skepper, J. N., Chatterjee, V. K., *et al.* (2009) Partial lipodystrophy and insulin resistant diabetes in a patient with a homozygous nonsense mutation in CIDEC. *EMBO Mol. Med.* **1,** 280–287 CrossRef Medline
29. Rajamoorthi, A., Arias, N., Basta, J., Lee, R. G., and Baldán, Á. (2017) Amelioration of diet-induced steatohepatitis in mice following combined therapy with ASO-Fsp27 and fenofibrate. *J. Lipid Res.* **58,** 2127–2138 CrossRef Medline
30. Rajamoorthi, A., Lee, R. G., and Baldán, Á. (2018) Therapeutic silencing of FSP27 reduces the progression of atherosclerosis in Ldlr(−/−) mice. *Atherosclerosis* **275,** 43–49 CrossRef Medline
31. Xu, W., Wu, L., Yu, M., Chen, F. J., Arshad, M., Xia, X., Ren, H., Yu, J., Xu, L., Xu, D., Li, J. Z., Li, P., and Zhou, L. (2016) Differential roles of cell death-inducing DNA fragmentation factor-alpha-like effector (CIDE) proteins in promoting lipid droplet fusion and growth in subpopulations of hepatocytes. *J. Biol. Chem.* **291,** 4282–4293 CrossRef Medline
32. Zhang, S., Shui, G., Wang, G., Wang, C., Sun, S., Zouboulis, C. C., Xiao, R., Ye, J., Li, W., and Li, P. (2014) Cidea control of lipid storage and secretion in mouse and human sebaceous glands. *Mol. Cell. Biol.* **34,** 1827–1838 CrossRef Medline
33. Keller, P., Petrie, J. T., De Rose, P., Gerin, I., Wright, W. S., Chiang, S. H., Nielsen, A. R., Fischer, C. P., Pedersen, B. K., and MacDougald, O. A. (2008) Fat-specific protein 27 regulates storage of triacylglycerol. *J. Biol. Chem.* **283,** 14355–14365 CrossRef Medline
34. Jambunathan, S., Yin, J., Khan, W., Tamori, Y., and Puri, V. (2011) FSP27 promotes lipid droplet clustering and then fusion to regulate triglyceride accumulation. *PLoS ONE* **6,** e28614 CrossRef Medline
35. Lee, S. M., Jang, T. H., and Park, H. H. (2013) Molecular basis for homodimerization of the CIDE domain revealed by the crystal structure of the CIDE-N domain of FSP27. *Biochem. Biophys. Res. Commun.* **439,** 564–569 CrossRef Medline
36. Bartz, R., Li, W. H., Venables, B., Zehmer, J. K., Roth, M. R., Welti, R., Anderson, R. G., Liu, P., and Chapman, K. D. (2007) Lipidomics reveals that adiposomes store ether lipids and mediate phospholipid traffic. *J. Lipid Res.* **48,** 837–847 CrossRef Medline
37. Chitraju, C., Trötzmuller, M., Hartler, J., Wolinski, H., Thallinger, G. G., Lass, A., Zechner, R., Zimmermann, R., Köfeler, H. C., and Spener, F. (2012) Lipidomic analysis of lipid droplets from murine hepatocytes reveals distinct signatures for nutritional stress. *J. Lipid Res.* **53,** 2141–2152 CrossRef Medline
38. Krahmer, N., Guo, Y., Wilfling, F., Hilger, M., Lingrell, S., Heger, K., Newman, H. W., Schmidt-Supprian, M., Vance, D. E., Mann, M., Farese, R. V., Jr., and Walther, T. C. (2011) Phosphatidylcholine synthesis for lipid droplet expansion is mediated by localized activation of CTP:phosphocholine cytidylyltransferase. *Cell Metab.* **14,** 504–515 CrossRef Medline
39. Barneda, D., Planas-Iglesias, J., Gaspar, M. L., Mohammadyani, D., Prasannan, S., Dormann, D., Han, G. S., Jesch, S. A., Carman, G. M., Kagan, V., Parker, M. G., Ktistakis, N. T., Klein-Seetharaman, J., Dixon, A. M., Henry, S. A., and Christian, M. (2015) The brown adipocyte protein CIDEA promotes lipid droplet fusion via a phosphatidic acid-binding amphipathic helix. *Elife* **4,** e07485 CrossRef Medline
40. Fei, W., Shui, G., Zhang, Y., Krahmer, N., Ferguson, C., Kapterian, T. S., Lin, R. C., Dawes, I. W., Brown, A. J., Li, P., Huang, X., Parton, R. G., Wenk, M. R., Walther, T. C., and Yang, H. (2011) A role for phosphatidic acid in the formation of "supersized" lipid droplets. *PLoS Genet.* **7,** e1002201 CrossRef Medline
41. Li, L., Shi, X., Guo, X., Li, H., and Xu, C. (2014) Ionic protein-lipid interaction at the plasma membrane: what can the charge do? *Trends Biochem. Sci.* **39,** 130–140 CrossRef Medline
42. Fairn, G. D., Schieber, N. L., Ariotti, N., Murphy, S., Kuerschner, L., Webb, R. I., Grinstein, S., and Parton, R. G. (2011) High-resolution mapping reveals topologically distinct cellular pools of phosphatidylserine. *J. Cell Biol.* **194,** 257–275 CrossRef Medline
43. Zhang, W., Crocker, E., McLaughlin, S., and Smith, S. O. (2003) Binding of peptides with basic and aromatic residues to bilayer membranes: phenylalanine in the myristoylated alanine-rich C kinase substrate effector domain penetrates into the hydrophobic core of the bilayer. *J. Biol. Chem.* **278,** 21459–21466 CrossRef Medline

44. Xu, C., Gagnon, E., Call, M. E., Schnell, J. R., Schwieters, C. D., Carman, C. V., Chou, J. J., and Wucherpfennig, K. W. (2008) Regulation of T cell receptor activation by dynamic membrane binding of the CD3ϵ cytoplasmic tyrosine-based motif. *Cell* **135,** 702–713 CrossRef Medline
45. Sengupta, P., Bosis, E., Nachliel, E., Gutman, M., Smith, S. O., Mihályné, G., Zaitseva, I., and McLaughlin, S. (2009) EGFR juxtamembrane domain, membranes, and calmodulin: kinetics of their interaction. *Biophys. J.* **96,** 4887–4895 CrossRef Medline
46. Kaadige, M. R., and Ayer, D. E. (2006) The polybasic region that follows the plant homeodomain zinc finger 1 of Pf1 is necessary and sufficient for specific phosphoinositide binding. *J. Biol. Chem.* **281,** 28831–28836 CrossRef Medline
47. Jack, E. R., Madine, J., Lian, L. Y., and Middleton, D. A. (2008) Membrane interactions of peptides representing the polybasic regions of three Rho GTPases are sensitive to the distribution of arginine and lysine residues. *Mol. Membr. Biol.* **25,** 14–22 CrossRef Medline
48. Gambhir, A., Hangyás-Mihályné, G., Zaitseva, I., Cafiso, D. S., Wang, J., Murray, D., Pentyala, S. N., Smith, S. O., and McLaughlin, S. (2004) Electrostatic sequestration of PIP2 on phospholipid membranes by basic/aromatic regions of proteins. *Biophys. J.* **86,** 2188–2207 CrossRef Medline
49. Murray, D. H., and Tamm, L. K. (2009) Clustering of syntaxin-1A in model membranes is modulated by phosphatidylinositol 4,5-bisphosphate and cholesterol. *Biochemistry* **48,** 4617–4625 CrossRef Medline
50. Thiam, A. R., Farese, R. V., Jr., and Walther, T. C. (2013) The biophysics and cell biology of lipid droplets. *Nat. Rev. Mol. Cell Biol.* **14,** 775–786 CrossRef Medline
51. Qian, H., Chen, Y., Nian, Z., Su, L., Yu, H., Chen, F. J., Zhang, X., Xu, W., Zhou, L., Liu, J., Yu, J., Yu, L., Gao, Y., Zhang, H., Zhang, H., *et al.* (2017) HDAC6-mediated acetylation of lipid droplet-binding protein CIDEC regulates fat-induced lipid storage. *J. Clin. Invest.* **127,** 1353–1369 CrossRef Medline
52. Heo, W. D., Inoue, T., Park, W. S., Kim, M. L., Park, B. O., Wandless, T. J., and Meyer, T. (2006) PI(3,4,5)P_3 and PI(4,5)P_2 lipids target proteins with polybasic clusters to the plasma membrane. *Science* **314,** 1458–1461 CrossRef Medline
53. Boroda, S., Takkellapati, S., Lawrence, R. T., Entwisle, S. W., Pearson, J. M., Granade, M. E., Mullins, G. R., Eaton, J. M., Villén, J., and Harris, T. E. (2017) The phosphatidic acid-binding, polybasic domain is responsible for the differences in the phosphoregulation of lipins 1 and 3. *J. Biol. Chem.* **292,** 20481–20493 CrossRef Medline
54. Aguilar, H. C., Matreyek, K. A., Choi, D. Y., Filone, C. M., Young, S., and Lee, B. (2007) Polybasic KKR motif in the cytoplasmic tail of Nipah virus fusion protein modulates membrane fusion by inside-out signaling. *J. Virol.* **81,** 4520–4532 CrossRef Medline
55. Modha, R., Campbell, L. J., Nietlispach, D., Buhecha, H. R., Owen, D., and Mott, H. R. (2008) The Rac1 polybasic region is required for interaction with its effector PRK1. *J. Biol. Chem.* **283,** 1492–1500 CrossRef Medline
56. Nian, Z., Sun, Z., Yu, L., Toh, S. Y., Sang, J., and Li, P. (2010) Fat-specific protein 27 undergoes ubiquitin-dependent degradation regulated by triacylglycerol synthesis and lipid droplet formation. *J. Biol. Chem.* **285,** 9604–9615 CrossRef Medline